Eur. Phys. J. B **52**, 23–36 (2006)
DOI: 10.1140/epjb/e2006-00273-y

THE EUROPEAN PHYSICAL JOURNAL B

Universal low-temperature behavior of frustrated quantum antiferromagnets in the vicinity of the saturation field

O. Derzhko[1,2,a] and J. Richter[2]

[1] Institute for Condensed Matter Physics, National Academy of Sciences of Ukraine, 1 Svientsitskii Street, L'viv-11, 79011, Ukraine
[2] Institut für Theoretische Physik, Universität Magdeburg, P.O. Box 4120, 39016 Magdeburg, Germany

Received 2 April 2006
Published online 6 July 2006 –

Abstract. We study the low-temperature thermodynamic properties of a number of frustrated quantum antiferromagnets which support localized magnon states in the vicinity of the saturation field. For this purpose we use (1) a mapping of the low-energy degrees of freedom of spin systems onto the hard-core object lattice gases and (2) an exact diagonalization of finite spin systems of up to $N = 30$ sites. The considered spin systems exhibit universal behavior which is determined by a specific hard-core object lattice gas representing the independent localized magnon states. We test the lattice gas description by comparing its predictions with the numerical results for low-lying energy states of finite spin systems. For all frustrated spin systems considered we find a strong variation of the low-temperature specific heat passing the saturation field and a maximum in the isothermal entropy at saturation field resulting in an enhanced magnetocaloric effect.

PACS. 75.10.Jm Quantized spin models – 75.45.+j Macroscopic quantum phenomena in magnetic systems – 75.30.Sg Magnetocaloric effect, magnetic cooling

1 Introductory remarks

Quantum spin antiferromagnets on geometrically frustrated lattices have attracted much attention during last years [1–3]. A new and rapidly developing direction in this field of quantum magnetism is a study of the low-temperature properties of such systems in the presence of an external magnetic field. The Zeeman interaction of spins with a magnetic field competes with the frustrating antiferromagnetic interspin interactions that may lead to new phenomena. Recently it has been found that a wide class of geometrically frustrated quantum spin antiferromagnets (including the kagomé and pyrochlore antiferromagnets) has quite simple ground states in the vicinity of the saturation magnetic field [4–6] (for a review, see Refs. [7,8]). These ground states consist of independent (i.e. isolated) localized magnons in a ferromagnetic environment. The localized magnon states were used to predict a ground-state magnetization jump at the saturation field [4–6], a magnetic field induced spin-Peierls instability [9,10], and a residual ground-state entropy at the saturation field [3,8,11–13]. Moreover, in references [8,12,13] the concept of localized magnons was used for a detailed analysis of the low-temperature magnetothermodynamics in the vicinity of the saturation field for two representative systems, the sawtooth chain (or Δ-chain) and the kagomé lattice. In particular, the authors of these papers mapped the low-energy degrees of freedom of the sawtooth chain (the kagomé lattice) to the hard-dimer gas on a one-dimensional lattice (the hard-hexagon gas on a triangular lattice) and used the results for the classical lattice gases to discuss the properties of the spin systems. They also provided exact diagonalization data for finite sawtooth chains (up to $N = 20$ sites) to illustrate the efficiency of the hard-dimer description of the spin chain at low temperatures near the saturation field.

In the present paper we extend the previous studies on the low-temperature strong-field magnetothermodynamics examining various other frustrated quantum spin antiferromagnets supporting localized magnon states. We emphasize that all such spin systems exhibit a universal behavior. It is determined by a specific hard-core object lattice gas which mimics the independent localized magnon states. Thus, the one-dimensional hard-dimer behavior is also inherent in the two-leg ladder or kagomé-like chains, whereas the hard-hexagon behavior is also inherent in the star lattice (see Tab. 1 below). Moreover, we

[a] e-mail: derzhko@icmp.lviv.ua

Table 1. Specific and generic properties of the spin systems shown in Figures 1 and 2. ϵ_1 is the difference between the energy of the fully polarized state and the energy of the one-magnon state in zero field and determines the saturation field $h_1 = \epsilon_1$, $n_{\max}$ is the maximum number of independent localized magnons for the closest possible packing, $\mathcal{N}$ is the number of sites in the auxiliary lattice with hard-core objects, N is the number of sites in the spin lattice.

Lattice	Relation between J_{ij}	ϵ_1	$n_{\max}/N$	$\mathcal{N}/N$	Universality class
Fig. 1a	$J_2 \geq 2J_1$	$2s(J_1+J_2)$	1/3	1/3	monomers
Fig. 1b	$J_3 \geq J_3^c(J_1,J_2)$; if $J_1 = J_2$ then $J_3 \geq ((1+\sqrt{5})/2)J_1$	$2s(J_1+J_3)$	1/4	1/4	monomers
Fig. 1c	$J_2 = 2J_1$	$8sJ_1$	1/4	1/2	dimers
Fig. 1d	$J_2 \geq 2J_1$	$2s(2J_1+J_2)$	1/4	1/2	dimers
Fig. 1e	all bonds have the same strength J	$6sJ$	1/6	1/3	dimers
Fig. 1f	$J_2 = (3/2)J_1$	$6sJ_1$	1/10	1/5	dimers
Fig. 2a	$J_2 \geq J_1$	$2s(J_1+2J_2)$	1/6	1/6	monomers
Fig. 2b	all bonds have the same strength J	$6sJ$	1/9	1/3	hexagons
Fig. 2c	all bonds have the same strength J	$5sJ$	1/18	1/6	hexagons
Fig. 2d	all bonds have the same strength J	$8sJ$	1/8	1/2	squares

examine the thermodynamic properties of the spin models which are described by a gas of monomers. We also provide exact diagonalization data for finite spin systems of up to $N = 30$ sites and discuss to what extent a hard-core object description can reproduce the properties of the spin systems. We compare analytical and numerical results for different one-dimensional lattices and for the two-dimensional square-kagomé lattice.

The remainder of the paper is organized as follows. In Section 2 we introduce the spin models to be discussed. In Section 3 we discuss a hard-core object description of the independent localized magnon states. We also consider how the lattice gas description can be extended for a wider temperature/field region. In Section 4 we present the exact diagonalization data for finite systems and compare them with the analytical predictions which follow from the hard-core object picture. We discuss briefly the effects of the localized magnons on the temperature dependence of the specific heat and the magnetocaloric effect near the saturation field. Finally, in Section 5 we summarize our findings.

2 Geometrically frustrated spin models and localized magnons

In this paper we consider several frustrated quantum spin lattices discussed so far in the literature by various authors, namely, the diamond chain [14], the dimer-plaquette chain [15], the sawtooth chain [16], the two-leg ladder [17], two kagomé-like chains [18,19] (Fig. 1), the square-kagomé lattice [20], the kagomé lattice [3,5,21], the star lattice [3,22], the checkerboard lattice [23] (Fig. 2). (Note that further models hosting localized magnons can be constructed.) The Hamiltonian of the system consisting of N antiferromagnetically interacting spins in a magnetic field h reads

$$H = \sum_{(ij)} J_{ij}\mathbf{s}_i \cdot \mathbf{s}_j - hS^z = \sum_{(ij)} J_{ij}\left(\frac{1}{2}\left(s_i^+ s_j^- + s_i^- s_j^+\right) + s_i^z s_j^z\right) - hS^z, \quad S^z = \sum_i s_i^z \tag{1}$$

with $\mathbf{s}_i^2 = s(s+1)$ and $J_{ij} > 0$. From references [3–7] we know that for certain relations between J_{ij} (see Tab. 1) all spin lattices shown in Figures 1 and 2 support localized magnon states which become relevant at strong magnetic fields. In what follows we fix the energy scale by setting either $J = 1$ (for systems with only one exchange integral) or $J_1 = 1$ (for systems with more than one exchange integral). For the diamond and dimer-plaquette chains and for the two-leg ladder the magnons may be localized on the vertical bonds (see panels a, b and d in Fig. 1), for the sawtooth chain the localized magnons may be trapped in a valley between two neighboring triangles (panel c in Fig. 1), whereas for other lattices the localized magnons may occupy the even polygons shown by fat lines in Figures 1, 2. The explicit expressions for the localized one-magnon state having the smallest possible region of localization read

$$|1\mathrm{lm}\rangle \propto \left(|s-1_1, s_2\rangle - |s_1, s-1_2\rangle\right)|s, \ldots, s\rangle$$

(panels a, b and d in Fig. 1),

$$|1\mathrm{lm}\rangle \propto \big(|s-1_1, s_2, s_3\rangle - 2|s_1, s-1_2, s_3\rangle + |s_1, s_2, s-1_3\rangle\big)|s, \ldots, s\rangle$$

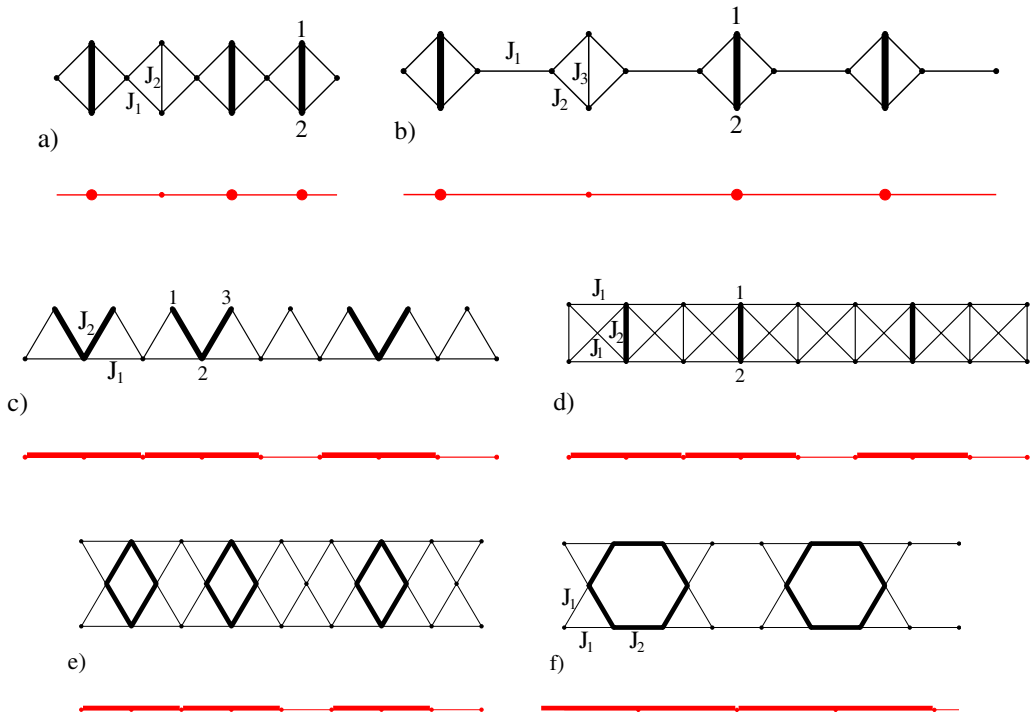

Fig. 1. (Color online) Several one-dimensional frustrated quantum spin lattices supporting localized magnon states: the diamond chain [14] (a), the dimer-plaquette chain [15] (b), the sawtooth chain [16] (c), the two-leg ladder (the spins are sitting only on the squares, not on the intersections of the diagonals) [17] (d), and two kagomé-like chains [18,19] (e and f). The trapping cells occupied by localized magnons are shown by fat lines. Below each lattice we show the corresponding auxiliary lattice filled by hard-core objects (monomers (a and b) and dimers (c, d, e and f)).

(panel c in Fig. 1),

$$|1\mathrm{lm}\rangle \propto \sum_m (-1)^m s_m^- |s,\ldots,s\rangle$$

(the sum over m runs, say, counterclockwise over the sites m of a trapping polygon in panels e and f in Fig. 1 and in all panels in Fig. 2). Here s_i or $s-1_i$ denote the values of s_i^z and s is the maximal possible value of s_i^z. We start with the zero-field case. The energy of the localized one-magnon state can be written as $E_{\rm FM}-\epsilon_1$, where $E_{\rm FM}$ is the energy of the fully (ferromagnetically) polarized spin system and the values of ϵ_1 for the considered systems are given in Table 1. We can fill the spin lattice by $n=1,\ldots,n_{\max}$, $n_{\max}\propto N$ (see Tab. 1) independent localized magnons. Each localized magnon decreases the magnetization S^z by 1 and the state with n localized magnons has $S^z=Ns-n$. The independent localized magnon states are the lowest-energy states in the corresponding sectors of $S^z=Ns-1,\ldots,Ns-n_{\max}$ [4,24]. Although the localized magnon states exist also for anisotropic XXZ Heisenberg exchange interaction in (1) and arbitrary spin length s, in what follows we restrict ourselves to the isotropic (i.e. XXX) Heisenberg exchange interaction and (in numerical computations) to the extreme quantum case $s=1/2$ without loss of generality for discussion of the universal low-temperature behavior of the spin systems near the saturation field. However, we have to bear in mind that the effects of the localized magnon states are true quantum effects which become less and less pronounced as $s\to\infty$ [5,11].

Consider now the localized magnon states in the presence of an external field h. A localized one-magnon state has the energy $E_1(h)=E_{\rm FM}-hsN-\epsilon_1+h$, whereas a state with n independent localized magnons has the energy

$$E_n(h)=E_{\rm FM}-hsN-n\,(\epsilon_1-h)\,. \qquad (2)$$

Evidently, n independent localized magnons can be placed on a lattice with N sites in many ways. We denote by $g_N(n)\geq 1$ the number of ways in which n independent localized magnons, each occupying the smallest possible area, can be put on a lattice with N sites. The energy of any of these $g_N(n)$ states is the same and is given by equation (2), i.e. $g_N(n)$ is the degeneracy of the independent localized n-magnon states. At the saturation field $h_1=\epsilon_1$ the energy $E_n(h_1)$ (2) does not depend on n that further increases the degeneracy of the independent localized magnon states.

Let us briefly recall the consequences of the localized magnons [3–13]. Due to the localized magnons different spin systems have identical/universal behavior in the ground state in strong magnetic fields. Since the

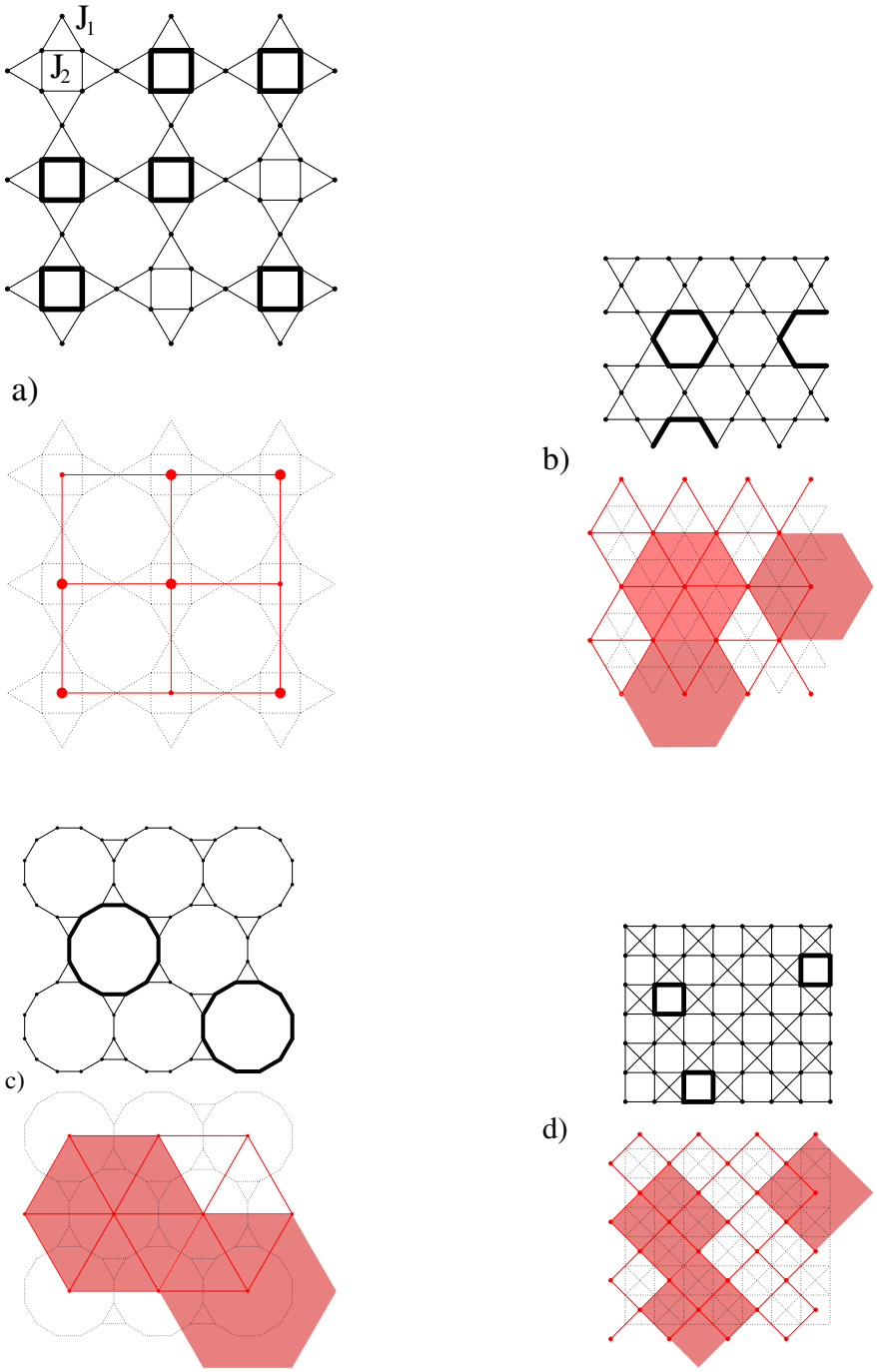

Fig. 2. (Color online) Several two-dimensional frustrated quantum spin lattices supporting localized magnon states: the square-kagomé lattice [20] (a), the kagomé lattice [3,5,21] (b), the star lattice [3,22] (c), and the checkerboard lattice (the spins are sitting only on the squares, not on the intersections of the diagonals) [23] (d). The trapping cells occupied by localized magnons are shown by fat lines. Below each lattice we show the corresponding auxiliary lattice (square (a and d) and triangular (b and c) lattices) filled by hard-core objects (monomers (a), hexagons (b and c) and squares (d)).

lowest-energy states with different numbers of independent localized magnons $n = 1, \ldots, n_{\max}$ have the same energy at the saturation field h_1, $E_{\rm FM} - h_1 sN$, the ground-state magnetization exhibits a jump at $h = h_1$ between the values Ns and $Ns - n_{\max}$. This jump is accompanied by a preceding plateau. Next, the ground-state energy at the saturation field exhibits a huge degeneracy which grows exponentially with the system size (at least as $2^{n_{\max}}$) and hence the ground-state entropy per site remains finite at $h = h_1$. Finally, a lattice distortion which preserves the symmetry of the cell which hosts a localized magnon may lower the total ground-state energy (which consists of the magnetic and elastic parts). This deformation, which obviously cannot exist for $h > h_1$, leads to a field-tuned ground-state structural instability in the vicinity of the saturation field.

One may expect that the contribution of localized magnons is dominant also at low temperatures and strong magnetic fields around the saturation field. The analysis for the sawtooth chain and the kagomé lattice reported in references [8,12,13] supports this expectation. We now move on to discuss the contribution of the independent localized magnons to the low-temperature properties of the considered spin systems in the vicinity of the saturation field.

3 Independent localized magnons and classical lattice gases

In this section, we examine the contribution of the independent localized magnons to the thermodynamic quantities of the spin systems. Moreover, we use for this purpose a hard-core object representation of the independent localized magnons of the smallest area. Such a representation allows us to utilize the broad knowledge on classical lattice gases. In the context of this approach a number of questions naturally arise which we have to consider. First, one has to show that the independent localized magnon states of smallest area are linearly independent in each sectors of $S^z = Ns-1,\ldots,Ns-n_{\max}$. Only in this case they all contribute to the partition function of the spin system. Although there is no proof of the linear independence of the independent localized magnons in the general case, this question has been discussed in references [8,13] and a rigorous proof for all spin systems shown in Figures 1, 2 is given in reference [25]. Thus, it was shown that for the diamond chain, the dimer-plaquette chain, the two-leg ladder, and the square-kagomé lattice (the orthogonal type of frustrated spin systems in the nomenclature of Ref. [25]) as well as for the sawtooth chain and two kagomé-like chains (the isolated type of frustrated spin systems) the independent localized magnon states are linearly independent in every sector of $S^z = Ns-1,\ldots,Ns-n_{\max}$. Moreover, for a system of the orthogonal type they form an orthogonal basis. The kagomé lattice, the star lattice and the checkerboard lattice belong to the frustrated spin systems of codimension one type. They possess exactly one nontrivial linear relation between their localized one-magnon states, but the set of n independent localized magnon states is linearly independent for $n = 2,\ldots,n_{\max}$ [25]. Thus, in the thermodynamic limit the linear independence of the localized magnons is fulfilled for all considered spin systems.

Next, we have to check that there are no other low-energy states (except the independent localized magnons) in every sector of $S^z = Ns-1,\ldots,Ns-n_{\max}$, or at least to show, if they do exist, that their contribution is vanishingly small in the thermodynamic limit. In references [8,13] it was shown that for the kagomé lattice there are indeed a few classes of states in the sectors $S^z = Ns-1,\ldots,Ns-n_{\max}$ which cannot be represented in terms of the independent localized magnons of smallest area. Thus, it remains unclear whether these additional states contribute to the partition function in the thermodynamic limit. In our numerical data (see Tabs. 2 and 3 below) we also find extra spin states for the diamond chain with $J_2 = 2J_1$, the square-kagomé lattice with $J_2 = J_1$, the two-leg ladder with $J_2 = 2J_1$ and two kagomé-like chains (but not for the diamond chain with $J_2 = 3J_1$, the dimer-plaquette chain with $J_2 = J_1$, $J_3 = 2J_1$, the square-kagomé lattice with $J_2 = 2J_1$, the sawtooth chain and the two-leg ladder with $J_2 = 3J_1$). For all these systems, except the square-kagomé lattice with $J_2 = J_1$, the numbers of the extra spin states do not increase with increasing of the lattice sizes that indicates their irrelevance in the thermodynamic limit. For the square-kagomé lattice with $J_2 = J_1$, as for the checkerboard [25] and the kagomé [26] lattices, we find much more extra spin states, however, our data restricted to finite systems are not sufficient to find reasonable tendencies for the thermodynamic limit. Furthermore, we have to discuss whether the independent localized magnon states are separated by a finite energy from higher-energy states. We postpone a discussion of this issue till Section 4 where the results of the exact diagonalization for finite systems are presented.

We are interested in the contribution of the independent localized magnons of smallest area to the thermodynamics of the spin systems. To find this contribution we must calculate the part of the partition function of the spin system, $Z(T,h,N) = \sum_j \exp\left(-E_j(h,N)/kT\right)$ (j denotes all states of the system of N spins s on a lattice), which comes from the independent localized magnons. Denoting this quantity by $Z_{\rm lm}(T,h,N)$ we have

$$Z_{\rm lm}(T,h,N) = \sum_{n=0}^{n_{\max}} g_N(n) \exp\left(-\frac{E_n(h)}{kT}\right) = \exp\left(-\frac{E_{\rm FM}-hsN}{kT}\right) \sum_{n=0}^{n_{\max}} g_N(n) \exp\Big(\frac{\mu}{kT} n\Big) \tag{3}$$

with $\mu = \epsilon_1 - h$.

An important step for further calculation of $Z_{\rm lm}(T,h,N)$ (3) is a mapping onto a hard-core object lattice gas. Consider an auxiliary lattice in which each site can be occupied or not by a hard-core object (monomer, dimer, hexagon or square) which corresponds to a localized magnon of smallest area (see Figs. 1, 2). Let us denote by $\mathcal{N}$ the number of sites of the auxiliary lattice; the relation between N and $\mathcal{N}$ for the considered spin systems is given in Table 1. We note that $g_N(n)$ is simply the canonical partition function $Z(n,\mathcal{N})$ of n hard-core objects placed on a lattice with $\mathcal{N}$ sites. Furthermore, $\Xi(T,\mu,\mathcal{N}) = \sum_n \exp(\mu n/kT) Z(n,\mathcal{N})$ is the grand canonical partition function of hard-core objects placed on a lattice with $\mathcal{N}$ sites and μ is the chemical potential. As a result, according to equation (3) we arrive at the basic relation between the thermodynamic quantities of independent localized magnons and hard-core models, i.e. $Z_{\rm lm}(T,h,N) = \exp(-(E_{\rm FM}-hsN)/kT)\Xi(T,\mu,\mathcal{N})$.

The calculation of $\Xi(T,\mu,\mathcal{N})$ for a classical hard-core object lattice gas (usually in the thermodynamic limit), in general, is a nontrivial problem [27]. It may be convenient to perform such calculations using the occupation number

representation. Let us introduce the occupation number n_i which takes two values, 0 and 1, depending whether the site i of the auxiliary lattice is empty or occupied, $i = 1, \ldots, \mathcal{N}$. Then the grand canonical partition function of hard-core objects can be rewritten in the following way

$$\Xi(T,\mu,\mathcal{N}) = \sum_{n_1=0,1} \ldots \sum_{n_\mathcal{N}=0,1} \exp\left(\frac{\mu}{kT}\sum_{i=1}^{\mathcal{N}} n_i\right) R(n_1,\ldots,n_\mathcal{N}), \quad (4)$$

where the function $R(n_1,\ldots,n_\mathcal{N}) \neq 1$ appears if the hard-core objects are extended (dimers, hexagons, squares) rather than simple monomers. For example, for the sawtooth chain, for which the corresponding hard-core objects are rigid dimers, we have $R(n_1,\ldots,n_\mathcal{N}) = \prod_i (1 - n_i n_{i+1})$ and all the terms in (4) which correspond to two adjacent sites of the auxiliary lattice being occupied have dropped out.

Using the relation between the independent localized magnons partition function $Z_{\rm lm}(T,h,N)$ and the grand canonical partition function of hard-core object lattice gas $\Xi(T,\mu,\mathcal{N})$ we get the following result for the Helmholtz free energy (per site) of the independent localized magnons

$$\frac{F_{\rm lm}(T,h,N)}{N} = \frac{E_{\rm FM}}{N} - hs - kT\frac{\ln \Xi(T,\mu,\mathcal{N})}{N}. \quad (5)$$

The entropy $S_{\rm lm}(T,h,N) = -\partial F_{\rm lm}(T,h,N)/\partial T$ and the specific heat $C_{\rm lm}(T,h,N) = T\partial S_{\rm lm}(T,h,N)/\partial T$ follow immediately from equation (5). We can also calculate the average number of hard-core objects $\langle n\rangle = \sum_{i=1}^{\mathcal{N}}\langle n_i\rangle = kT\partial \ln \Xi(T,\mu,\mathcal{N})/\partial\mu$ which yields the magnetization $\langle S^z\rangle_{\rm lm} = sN - \langle n\rangle$.

Next, we turn to the specific lattice gases which are related to the considered spin systems. Although the results for various lattice gases are not new and can be found in the literature [27] we present some of them here for easy references in view of further discussions for the spin systems.

3.1 Monomers

The independent localized magnon states in the diamond and dimer-plaquette chains as well as in the square-kagomé lattice can be mapped onto a lattice gas of monomers (see panels a and b in Fig. 1, panel a in Fig. 2 and Tab. 1). The calculation of the thermodynamic quantities for the lattice gas of monomers is simple. We have $Z(n,\mathcal{N}) = \mathcal{C}^n_\mathcal{N} = \mathcal{N}!/(n!(\mathcal{N}-n)!)$, $\Xi(T,\mu,\mathcal{N}) = \sum_{n=0}^{\mathcal{N}} \mathcal{C}^n_\mathcal{N} \exp(\mu n/kT) = (\exp(\mu/kT)+1)^\mathcal{N}$ or, using equation (4), $\Xi(T,\mu,\mathcal{N}) = (\sum_{n=0,1}\exp(\mu n/kT))^\mathcal{N} = (1+\exp(\mu/kT))^\mathcal{N}$. The Helmholtz free energy of the gas of monomers reads

$$\frac{F_{\rm lm}(T,h,N)}{N} = \frac{E_{\rm FM}}{N} - hs - \frac{\mathcal{N}}{N}kT\ln\left(1+\exp\frac{\mu}{kT}\right) \quad (6)$$

and therefore

$$\frac{S_{\rm lm}(T,h,N)}{kN} = \frac{\mathcal{N}}{N}\left(\ln(1+\exp x) - \frac{x\exp x}{1+\exp x}\right), \quad (7)$$

$$\frac{C_{\rm lm}(T,h,N)}{kN} = \frac{\mathcal{N}}{N}\frac{\left(\frac{x}{2}\right)^2}{\cosh^2\frac{x}{2}}, \quad (8)$$

$$\frac{\langle S^z\rangle_{\rm lm}}{sN} = 1 - \frac{1}{s}\frac{\mathcal{N}}{N}\frac{\exp x}{1+\exp x} \quad (9)$$

with $x = \mu/kT$. Equations (7, 8) are symmetric with respect to $x \to -x$. We note that at saturation $\mu = 0$ and equation (7) yields $S_{\rm lm}(T,h_1,N)/kN = (\mathcal{N}/N)\ln 2$. That is the value of the residual entropy per site obtained earlier for the diamond and dimer-plaquette chains [11]. The specific heat $C_{\rm lm}(T,h,N)/k\mathcal{N}$, equation (8), exhibits two symmetric maxima of height $C_{\max} \approx 0.43922884$ at $x \approx \pm 2.39935728$. The universal dependences of $(Ns - \langle S^z\rangle_{\rm lm})/\mathcal{N}$, equation (9), of $S_{\rm lm}/k\mathcal{N}$, equation (7), and of $C_{\rm lm}/k\mathcal{N}$, equation (8), are shown in Figures 3, 4 (for a more detailed discussion of these figures, see Sect. 4).

We may consider an improvement of a lattice gas description of low-lying energy levels of spin systems taking into account higher-energy states which are separated from the hard-core object states by a gap. According to equation (4) within a lattice gas model there are only two states at each lattice site. Namely, the site may be either empty ($n_i = 0$) and such a state occurs with the probability $\propto 1$, or the site may be occupied by monomer ($n_i = 1$) and such a state occurs with the probability $\propto \exp(\mu/kT)$. We may increase the number of states at each sites introducing an additional higher-energy state of monomers which occurs with the probability $\propto \exp((\mu - U)/kT)$ and U is large positive on-site energy. Obviously, if $U \to \infty$ the higher-energy states are irrelevant, but for finite U they become relevant as temperature grows. In the spin picture, the second state corresponds to a higher-energy state with a wave function located in the area which is mapped onto one site of the auxiliary lattice. Our calculations confirm that the made assumption really yields an improvement for higher temperatures (see the corresponding panels in Figs. 3, 7, 8). The grand partition function of the modified lattice-gas model can be easily calculated

$$\Xi(T,\mu,\mathcal{N}) = \left(1 + \exp\frac{\mu}{kT} + \exp\frac{\mu - U}{kT}\right)^\mathcal{N}. \quad (10)$$

From equation (10) we find the entropy, the specific heat, and the magnetization using usual thermodynamic relations. The corresponding results are illustrated in Figures 3, 7, 8 assuming values for U related to the energy separation between the localized magnon states and higher-energy states for finite spin lattices, see Section 4. The improved approximation agrees with exact diagonalization results up to higher temperatures in comparison with the monomer lattice gas predictions (6)–(9).

3.2 One-dimensional dimers

The independent localized magnons in the sawtooth chain, the two-leg ladder and two kagomé-like chains can be

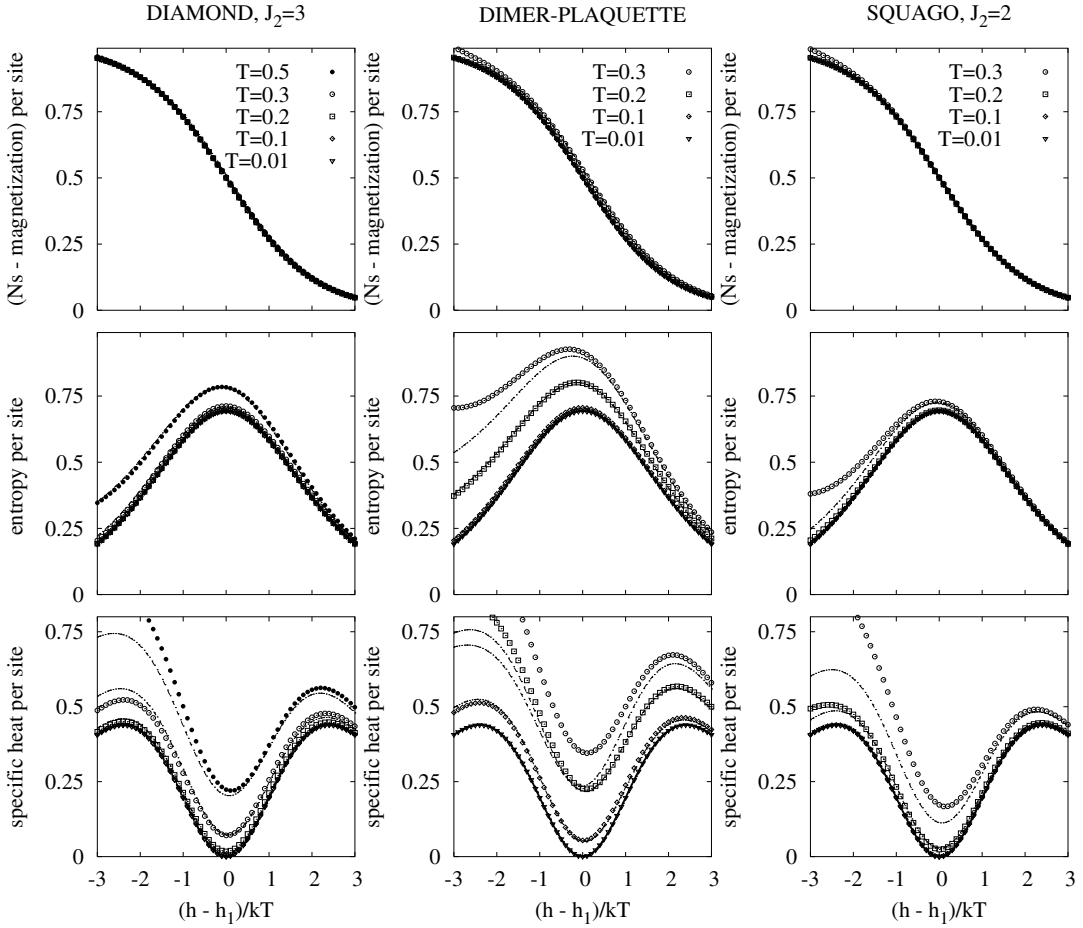

Fig. 3. The universal dependences of $(sN-\langle S^z\rangle_{\rm lm})/\mathcal{N}$ (9), $S_{\rm lm}/k\mathcal{N}$ (7) and $C_{\rm lm}/k\mathcal{N}$ (8) (monomer universality class) together with the corresponding results for finite spin systems (diamond chain with $N=18$, $J_1=1$, $J_2=3$ [left column], dimer-plaquette chain with $N=20$, $J_1=J_2=1$, $J_3=2$ [middle column], square-kagomé lattice with $N=18$, $J_1=1$, $J_2=2$ [right column]). The universal dependences are shown by solid lines, the exact diagonalization data are shown by symbols. Note that the exact diagonalization data for the lowest temperature coincide with the universal dependences for monomers. We also show by thin broken lines the analytical results which follow from (10) with $U=1.57,\ 0.58,\ 1.34$ for the diamond chain, dimer-plaquette chain and square-kagomé lattice, respectively, which are in good agreement with numerical data for higher temperatures.

mapped onto a one-dimensional lattice gas of rigid dimers (see panels c, d, e, f in Fig. 1 and Tab. 1). The grand partition function $\Xi(T,\mu,\mathcal{N})$ (4) of rigid dimers on a chain of $\mathcal{N}$ sites with periodic boundary conditions can be calculated using the transfer-matrix method. The resulting expression for $\Xi(T,\mu,\mathcal{N})$ reads

$$\Xi(T,\mu,\mathcal{N})=\lambda_1^{\mathcal{N}}+\lambda_2^{\mathcal{N}},\quad \lambda_{1,2}=\frac{1}{2}\pm\sqrt{\frac{1}{4}+\exp\frac{\mu}{kT}}. \quad (11)$$

In the thermodynamic limit $\mathcal{N}\to\infty$ only the larger eigenvalue of the transfer matrix plays role in (11) and we have

$$\frac{F_{\rm lm}(T,h,N)}{N}=\frac{E_{\rm FM}}{N}-hs -\frac{\mathcal{N}}{N}kT\ln\left(\frac{1}{2}+\sqrt{\frac{1}{4}+\exp\frac{\mu}{kT}}\right). \quad (12)$$

For the entropy, specific heat, and magnetization we find from equation (12)

$$\frac{S_{\rm lm}(T,h,N)}{kN}=\frac{\mathcal{N}}{N}\left(\ln\left(\frac{1}{2}+\sqrt{\frac{1}{4}+\exp x}\right) -x\left(\frac{1}{2}-\frac{1}{4\sqrt{\frac{1}{4}+\exp x}}\right)\right), \quad (13)$$

$$\frac{C_{\rm lm}(T,h,N)}{kN}=\frac{\mathcal{N}}{N}\frac{x^2\exp x}{8\left(\frac{1}{4}+\exp x\right)^{\frac{3}{2}}}, \quad (14)$$

$$\frac{\langle S^z\rangle_{\rm lm}}{sN}=1-\frac{1}{s}\frac{\mathcal{N}}{N}\left(\frac{1}{2}-\frac{1}{4\sqrt{\frac{1}{4}+\exp x}}\right), \quad (15)$$

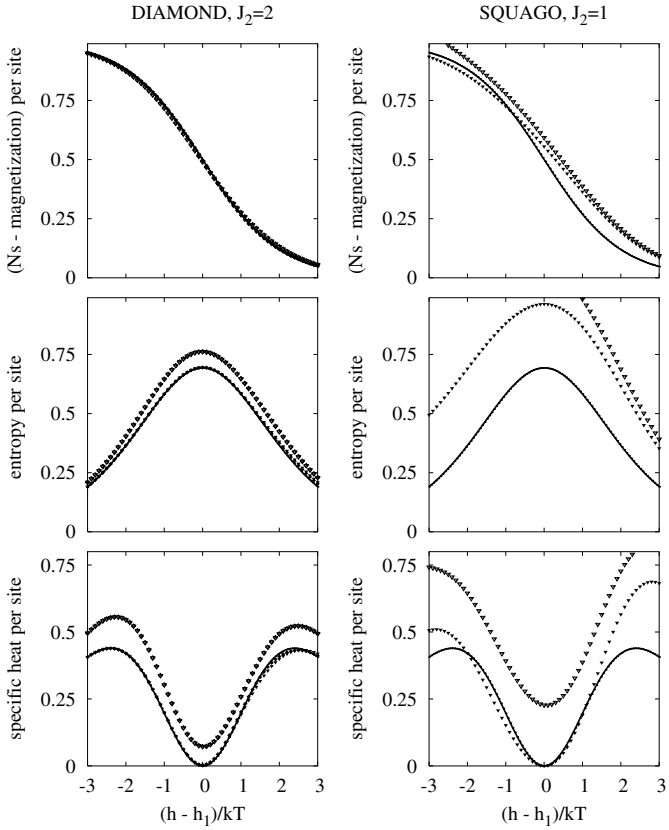

Fig. 4. The universal dependences for monomers (solid lines) of $(sN - \langle S^z\rangle_{\rm lm})/\mathcal{N}$, $S_{\rm lm}/k\mathcal{N}$ and $C_{\rm lm}/k\mathcal{N}$ together with the corresponding results for finite spin systems belonging to the monomer universality class but which have extra (not hard-monomer) spin states: the diamond chain with $N = 18$, $J_1 = 1$, $J_2 = 2$ (left column), the square-kagomé lattice with $N = 18$, $J_1 = J_2 = 1$ (right column). The numerical results for spin systems are shown for temperatures $kT = 0.01$ (filled symbols) and $kT = 0.1$ (empty symbols).

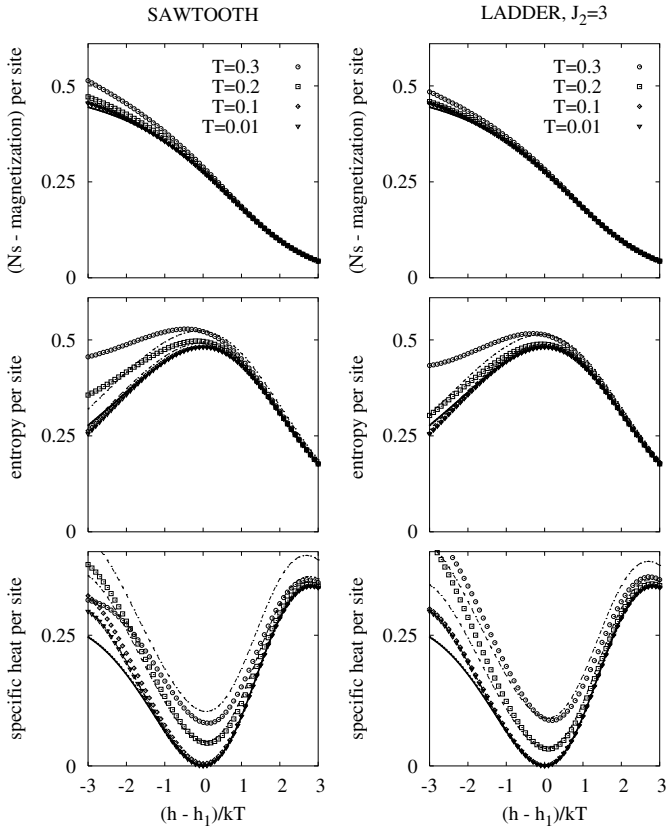

Fig. 5. The universal dependences of $(sN - \langle S^z\rangle_{\rm lm})/\mathcal{N}$, $S_{\rm lm}/k\mathcal{N}$ and $C_{\rm lm}/k\mathcal{N}$ (one-dimensional dimer universality class) together with the corresponding results for finite spin systems (sawtooth chain with $N = 20$, $J_1 = 1$, $J_2 = 2$ [left column] and two-leg ladder with $N = 20$, $J_1 = 1$, $J_2 = 3$ [right column]). The universal dependences which follow from (11) are shown by thick solid ($\mathcal{N} \to \infty$) and dashed lines ($\mathcal{N} = 10$), the exact diagonalization data are shown by symbols. Note that the exact diagonalization data for the lowest temperature coincide with the universal dependences for dimers. We also show by thin broken lines the analytical results which follow from (18) for $\mathcal{N} = 10$ with $U = 1.00$ and 1.10 for the sawtooth chain and two-leg ladder, respectively, which are in good agreement with numerical data for higher temperatures.

respectively. Note that equations (13, 14) are not symmetric with respect to $x \to -x$. Equations (13–15) were examined in references [8,12,13] in the context of the sawtooth chain. We also note that at saturation, i.e. at $\mu = 0$, equation (13) gives the values of the residual entropy per site for the kagomé-like chains and the two-leg ladder, $S_{\rm lm}(T, h_1, N)/kN = (\mathcal{N}/N)\ln((1+\sqrt{5})/2)$ [11]. The universal dependences $(Ns - \langle S^z\rangle_{\rm lm})/\mathcal{N}$, equation (15), $S_{\rm lm}/k\mathcal{N}$, equation (13), and $C_{\rm lm}/k\mathcal{N}$, equation (14), are shown in Figures 5 and 6 (for a more detailed discussion of these figures, see Sect. 4). The specific heat $C_{\rm lm}(T, h, N)/k\mathcal{N}$ exhibits two maxima of heights $C_{\rm max}^{\rm right} \approx 0.34394234$ and $C_{\rm max}^{\rm left} \approx 0.26887020$ at $(h - h_1)/kT \approx 2.81588498$ and $(h - h_1)/kT \approx -4.05258891$, respectively.

Again we may consider an improvement of a lattice gas description of the low-lying energy levels of spin systems. One way to consider higher-energy states was suggested by Zhitomirsky and Tsunetsugu [8]. These authors treat the factor $1 - n_i n_{i+1}$ in (4), as the $V \to \infty$ limit of a generalized factor $\exp(-(V/kT)n_i n_{i+1}) = 1 + (\exp(-V/kT) - 1)n_i n_{i+1}$. We may relax the hard-core restriction assuming the intersite interaction V to be large but finite and approximately equal to the energy separation between the localized magnon states and higher-energy states (in Ref. [8] the energy gap was also estimated using variational calculations). As a result, we arrive at a one-dimensional lattice gas with a finite nearest-neighbor repulsion. The grand partition function of such a gas is calculated by the transfer-matrix method and reads

$$\Xi(T,\mu,\mathcal{N}) = \lambda_1^{\mathcal{N}} + \lambda_2^{\mathcal{N}},$$
$$\lambda_{1,2} = \frac{1}{2} + \frac{1}{2}\exp\frac{\mu - V}{kT} \pm \sqrt{\frac{1}{4} + \exp\frac{\mu}{kT} - \frac{1}{2}\exp\frac{\mu - V}{kT} + \frac{1}{4}\exp\frac{2(\mu - V)}{kT}}. \quad (16)$$

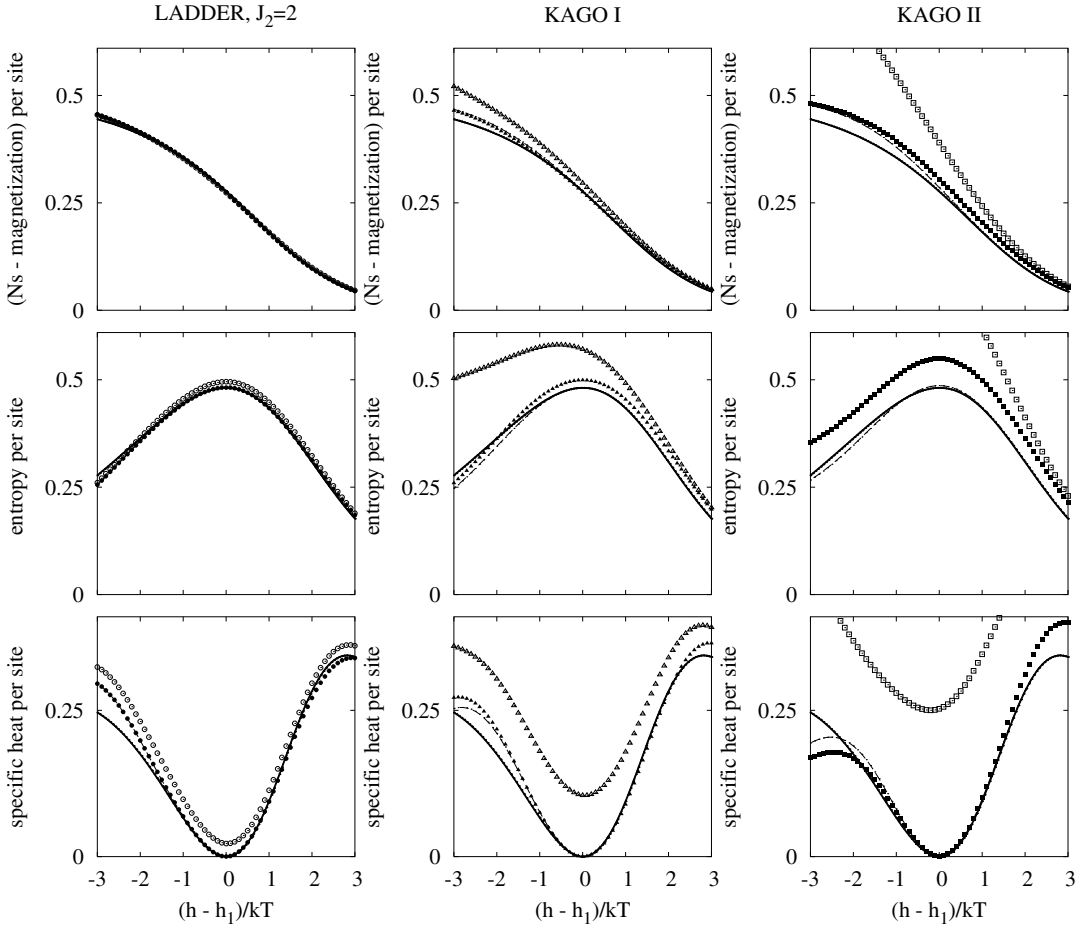

Fig. 6. The universal dependences of $(sN-\langle S^z\rangle_{\rm lm})/\mathcal{N}$, $S_{\rm lm}/k\mathcal{N}$ and $C_{\rm lm}/k\mathcal{N}$ for one-dimensional dimers ($\mathcal{N}\to\infty$ — thick solid lines; finite $\mathcal{N}$ — dashed lines) together with the corresponding results for finite spin systems belonging to the one-dimensional dimer universality class but which have extra (not hard-dimer) spin states: the two-leg ladder with $N=20$ (corresponds to $\mathcal{N}=10$), $J_1=1$, $J_2=2$ (left column), the kagomé-like chain shown in Figure 1e with $N=18$ (corresponds to $\mathcal{N}=6$), $J=1$ (middle column) and the kagomé-like chain shown in Figure 1f with $N=20$ (corresponds to $\mathcal{N}=4$), $J_1=1$ (right column). The numerical results for spin systems are shown for temperatures $kT=0.01$ (filled symbols) and $kT=0.1$ (empty symbols).

The thermodynamic quantities which follow from equation (16) are in a good agreement with exact diagonalization data for the sawtooth chain up to higher temperatures in comparison with the predictions in the $V\to\infty$ limit [8]. In the spin picture a finite V corresponds to higher-energy states with wave functions located on the areas which are mapped onto two adjacent sites of the auxiliary one-dimensional lattice. In addition, we can consider a similar improvement as for the monomer problem, namely we can assume additional higher-energy states of dimers which occur with the probability $\propto\exp((\mu-U)/kT)$, where U is positive and large. That means that more than one dimer is allowed on the same site, but that cost additional energy U. In the spin picture, we take into account a higher-energy state with a wave function located in the area which is mapped onto one site of the auxiliary one-dimensional lattice. Thus, combining the assumption about higher-energy state of dimer at each site and the weakening of the hard-core restriction we arrive at the following formula for the grand partition function

$$\Xi(T,h,\mathcal{N})=\lambda_1^{\mathcal{N}}+\lambda_2^{\mathcal{N}}+\lambda_3^{\mathcal{N}},$$
$$\lambda^3-\left(1+\exp\frac{\mu-V}{kT}\right)\lambda^2-\exp\frac{\mu}{kT}\left(1+\exp\left(-\frac{U}{kT}\right)-\exp\left(-\frac{V}{kT}\right)\right)\lambda+\exp\frac{2\mu-U-V}{kT}=0; \qquad (17)$$

in the thermodynamic limit $\mathcal{N}\to\infty$ only the largest root of the cubic equation enters the thermodynamic quantities. In the limit $U\to\infty$ equation (17) transforms into equation (16). In what follows we consider only the other limit $V\to\infty$ when equation (17) becomes

$$\Xi(T,\mu,\mathcal{N})=\lambda_1^{\mathcal{N}}+\lambda_2^{\mathcal{N}},$$
$$\lambda_{1,2}=\frac{1}{2}\pm\sqrt{\frac{1}{4}+\exp\frac{\mu}{kT}+\exp\frac{\mu-U}{kT}}. \qquad (18)$$

From equation (18) we find in a usual way the entropy, the specific heat, and the magnetization, which are shown

in Figures 5, 7, 8 assuming values for U again obtained by inspection of the energy spectrum of finite spin lattices (for more details see Sect. 4).

3.3 Hexagons on a triangular lattice and squares on a square lattice

For completeness we give here some remarks on the two-dimensional lattice gases of hard-core objects which emerge in the context of localized magnons in some two-dimensional frustrated quantum antiferromagnets. Such lattice gases are much more complicated subject for rigorous analytical or numerical studies.

For the kagomé and star lattices the independent localized magnons of smallest area can be put in correspondence to the hard hexagons on a triangular lattice (see panels b and c in Fig. 2 and Tab. 1). The grand canonical partition function for the hard hexagons on triangular lattice, $\Xi(T,\mu,\mathcal{N})$, was found by Baxter (hard-hexagon problem, see Ref. [27]). The parametric dependence of $(\Xi(T,\mu,\mathcal{N}))^{1/\mathcal{N}}$ on the activity $z = \exp(\mu/kT)$ in the thermodynamic limit $\mathcal{N} \to \infty$ can be found in reference [27]. The peculiarity of the hard-hexagon model is the existence of a phase transition at a critical value of activity $z_c = (11 + 5\sqrt{5})/2 \approx 11.09016994$ ($x_c = \ln z_c \approx 2.40605913$). The low-activity phase is uniform (liquid) with identical average occupation numbers of hexagons on each of three triangular sublattices, $n_1 = n_2 = n_3$, whereas the high-activity phase is nonuniform (solid) with $n_1 > n_2 = n_3$. The value of the entropy per site at $z = 1$ is $0.33324272k$; this number gives the residual entropy per site due to localized magnon states of smallest area for the kagomé and star lattices [8,11,13]. The hard-hexagon problem in the context of the low-temperature magnetothermodynamics of the kagomé lattice in the vicinity of the saturation field was discussed in detail in references [8,13].

For the checkerboard lattice the independent localized magnons of smallest area can be put in correspondence to the hard-core squares on a square lattice, where the size of the hard squares corresponds to the nearest-neighbor and the next-nearest-neighbor exclusions (see panel d in Fig. 2 and Tab. 1). We are not aware for an exact analytical solution of such a model, but approximative results are available [28]. In the context of the low-temperature magnetothermodynamics of the checkerboard lattice in the vicinity of the saturation field the hard-square problem has been discussed recently in reference [29]. The value of the entropy per site at $z = 1$ obtained applying a combination of the transfer-matrix calculations and Monte Carlo is about $0.2946k$ [29] (a direct calculation for periodic 8×8 (8×10) lattice yields about $0.2949k$ ($0.2948k$) [30]).

4 Exact diagonalization versus hard-core object description

After presenting explicit expressions for the thermodynamic quantities by using the correspondence between the localized magnon states of the quantum spin system and a classical hard-core description we now test our analytical results by comparison with finite-lattice numerical results of the full spin-1/2 system. Note that the classical equations for the monomer problem, see Section 3.1, do not depend on the size of the system, whereas the corresponding classical equations for the dimer problem, see Section 3.2, are size dependent. For the number of degenerate states presented in Tables 2 and 3 we could consider systems of up to $N = 30$ spins, since we can restrict the calculation of sectors with high total S^z. For the thermodynamics we used the data of full diagonalization of spin systems of either $N = 18$ or $N = 20$. For the estimation of the temperature and field ranges, in which the hard-core description is valid, and also for the estimation of the on-site energy parameter U, see Sections 3.1 and 3.2, it is useful to find a measure for the thermodynamically relevant energy separation Δ between the localized magnon states and the other eigenstates of the spin system. For that we have calculated the integrated low-energy density of states at saturation field and define Δ as that energy value above the localized magnon ground-state energy, where the contribution of the higher-energy states to the integrated density of states becomes as large as the contribution of the localized-magnon states.

In Figures 3 and 4 we present the results for the magnetization $(Ns - \langle S^z \rangle)/\mathcal{N}$, the entropy $S/k\mathcal{N}$, the specific heat $C/k\mathcal{N}$ in dependence on $(h-h_1)/kT$ for spin systems belonging to the monomer universality class, i.e. for the diamond chain, the dimer-plaquette chain and the square-kagomé lattice. Note that the universal formulas (6)–(9) depend only on $(h - h_1)/kT$, i.e. they are identical for all temperatures $kT = 0.01,\ 0.1,\ 0.2,\ 0.3,\ 0.5$ considered in Figures 3 and 4.

Figure 3 corresponds to spin systems, for which the number of degenerate spin states at the saturation $\mathcal{W}_{\rm sp}$ equals the number of states of the corresponding hard-core object lattice gas $\mathcal{W}$, see Table 2. Furthermore, these spin systems exhibit a quite large energy separation Δ. We find $\Delta \approx 1.5$ for the diamond chain ($J_1 = 1$, $J_2 = 3$, $N = 18$), $\Delta \approx 0.6$ for the dimer-plaquette chain ($J_1 = J_2 = 1$, $J_3 = 2$, $N = 20$), and $\Delta \approx 1.5$ for the square-kagomé lattice ($J_1 = 1$, $J_2 = 2$, $N = 18$). Obviously, in Figure 3 the curves for the spin systems at temperatures up to $kT \approx 0.1 \approx 0.1\Delta$ are almost identical with the universal curves. But also for $kT > 0.1$ the qualitative behavior of the entropy, the specific heat, and the magnetization is quite well modeled by the universal formulas (7–9). The modified lattice-gas model, see equation (10), with parameters U related to Δ indeed leads to an improved quantitative agreement with the results for the spin systems at higher temperatures.

Figure 4 corresponds to spin systems, for which the number of degenerate spin states at the saturation field $\mathcal{W}_{\rm sp}$ is larger than the number of states of the corresponding hard-core object lattice gas $\mathcal{W}$, see Table 2. However, for the diamond chain with $J_2 = 2J_1$, we have only one extra spin state, $\mathcal{W}_{\rm sp} = \mathcal{W} + 1$, which becomes irrelevant for larger N. By contrast, there is a noticeable disagreement

Table 2. Number of degenerate states: lattice gas of monomers and spin systems. For a gas of monomers on $\mathcal{N}$ sites we have $\mathcal{W} = \Xi(T, \mu = 0, \mathcal{N}) = 2^{\mathcal{N}}$.

$\mathcal{N}$	$\mathcal{W}$	Diamond ($J_2 = 2J_1$)	Diamond ($J_2 = 3J_1$)	Dimer-plaquette ($J_3 = 2J_1$)	Square-kagomé ($J_2 = J_1$)	Square-kagomé ($J_2 = 2J_1$)
3	8	9	8	8	18	8
4	16	17	16	16	42	16
5	32	33	32	32	52	32
6	64	65	64	64	–	–
7	128	129	128	–	–	–
8	256	257	256	–	–	–

Table 3. Number of degenerate states: one-dimensional hard-dimer lattice gas and spin systems. For one-dimensional dimer gas on $\mathcal{N}$ sites we have $\mathcal{W} = \Xi(T, \mu = 0, \mathcal{N}) = \lambda_1(\mu = 0)^{\mathcal{N}} + \lambda_2(\mu = 0)^{\mathcal{N}}$. Since $\lambda_1(\mu = 0) = \Phi$ is the golden number and $\lambda_2(\mu = 0) = 1 - \Phi = -1/\Phi$ we may use the properties of powers of Φ and its reciprocal. Namely, for any even integer n $\Phi^n + 1/\Phi^n$ is a whole number; in particular, 2, 3, 7, 18, 47, 123, 322 for $n = 0$, 2, 4, 6, 8, 10, 12. (For any odd integer n $\Phi^n - 1/\Phi^n$ is a whole number; in particular, 1, 4, 11, 29, 76, 199 for $n = 1$, 3, 5, 7, 9, 11.) See: `http://goldennumber.net/phipower.htm`

$\mathcal{N}$	$\mathcal{W}$	Sawtooth	Two-leg ladder ($J_2 = 2J_1$)	Two-leg ladder ($J_2 = 3J_1$)	Kagomé-like, Figure 1e	Kagomé-like, Figure 1f
4	7	7	8	7	9	9
6	18	18	19	18	20	20
8	47	47	48	47	49	–
10	123	123	124	123	–	–
12	322	322	323	322	–	–

between $\mathcal{W}_{\rm sp}$ and $\mathcal{W}$ for the square-kagomé lattice with $J_2 = J_1$ (Tab. 2). Similarly to the kagomé [8,13,26] and the checkerboard [25] lattices, for the square-kagomé lattice with $J_2 = J_1$ we have extra spin states which are not covered by the hard-core description illustrated in Section 3.1. The number of these extra spin states depends on system size N. From our numerical data for $N = 18,\ 24,\ 30$ we are not able to conclude whether the localized magnon states of smallest area dominate the low-temperature thermodynamics in the thermodynamic limit. Moreover, for these systems with extra spin states we estimate significantly lower separations Δ of higher-energy states, namely $\Delta \approx 0.3$ for the diamond chain ($J_1 = 1$, $J_2 = 2$, $N = 18$) and $\Delta \approx 0.2$ for the square-kagomé lattice ($J_1 = 1$, $J_2 = 1$, $N = 18$). As a consequence we may find (see Fig. 4) a perfect agreement between the spin and the hard-core data only for very low temperatures, but realize a quantitative deviation already for $kT \approx 0.1$. For the square-kagomé lattice with $J_1 = 1$, $J_2 = 1$ the larger number of extra spin states leads to a more pronounced deviation from the universal formulas. Nevertheless, the numerical data illustrate that the localized magnon states of smallest area contribute substantially to the partition function thus leading to a low-temperature behavior which is at least qualitatively in agreement with the universal behavior given by equations (7–9).

Next, we discuss the results for the magnetization $(Ns - \langle S^z \rangle)/\mathcal{N}$, the entropy $S/k\mathcal{N}$ and the specific heat $C/k\mathcal{N}$ in dependence on $(h - h_1)/kT$ for spin systems belonging to the dimer universality class, i.e. for the sawtooth chain, the frustrated two-leg ladder and the kagomé-like chains of type I and II, see Figures 5 and 6. Again, the universal formulas (11)–(15) depend only on $(h - h_1)/kT$, i.e. they are identical for all temperatures $kT = 0.01,\ 0.1,\ 0.2,\ 0.3$ considered in Figures 5 and 6. However, as mentioned already above, they are size dependent. Hence, we compare the spin data for systems of finite size N with the hard-core data of corresponding size $\mathcal{N}$ (cf. Tab. 1) obtained from equation (11). Note, however, that the systems considered in Figures 5 and 6, left panel, correspond to $\mathcal{N} = 10$, where the curves for the finite hard-dimer system are already close to those for the thermodynamic limit.

The results shown in Figure 5 belong to systems with no extra spin states, i.e. $\mathcal{W}_{\rm sp} = \mathcal{W}$, see Table 3, and quite large energy separation $\Delta \approx 0.8$ (sawtooth chain, $N = 18$) and $\Delta \approx 0.9$ (two-leg ladder, $J_1 = 1$, $J_2 = 3$, $N = 20$). Consequently, we find an excellent agreement between the spin data and the hard-dimer data for temperatures up to $kT \approx 0.1 \approx 0.1\Delta$. For larger temperatures again the qualitative behavior is well described by the universal formulas derived from equation (11). The modified hard-core description based on equation (18) with appropriate parameters U leads to a further quantitative improvement, see Figure 5.

Figure 6 corresponds to spin systems, for which the number of degenerate spin states $\mathcal{W}_{\rm sp}$ at the saturation field for finite spin systems is larger than the number of states $\mathcal{W}$ of corresponding finite hard-core object lattice gas, see Table 3. However, we have only one (two-leg ladder, $J_1 = 1$, $J_2 = 2$) or two (kagomé-like chains I and

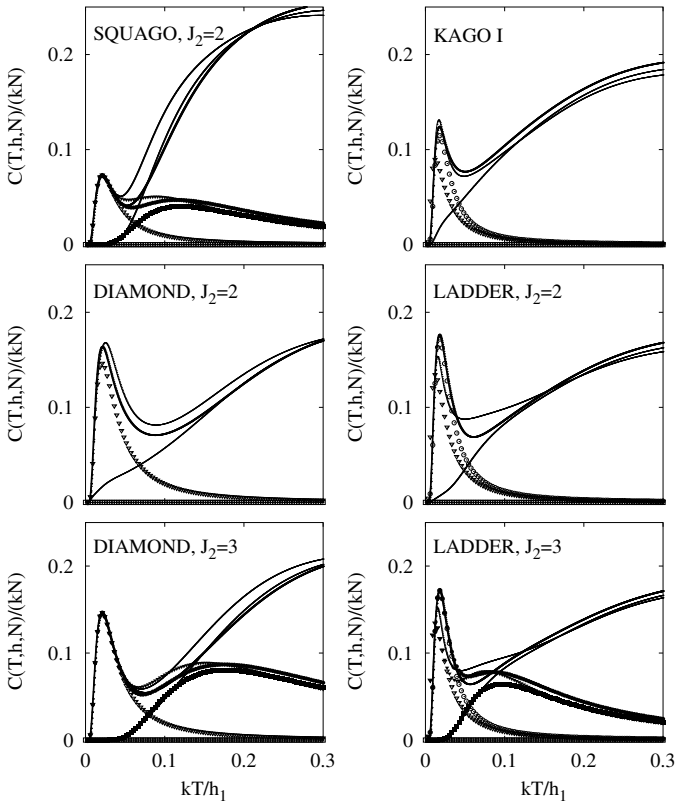

Fig. 7. The temperature dependences of the specific heat C/kN vs. kT/h_1 for several finite spin systems. Monomer universality class: left panels, from bottom to top, the diamond chain with $J_1 = 1$, $J_2 = 3$, $N = 18$, the diamond chain with $J_1 = 1$, $J_2 = 2$, $N = 18$, the square-kagomé lattice $J_1 = 1$, $J_2 = 2$, $N = 18$. One-dimensional dimer universality class: right panels, from bottom to top, the two-leg ladder with $J_1 = 1$, $J_2 = 3$, $N = 20$, the two-leg ladder with $J_1 = 1$, $J_2 = 2$, $N = 20$, the kagomé-like chain shown in Figure 1e with $J = 1$, $N = 18$. The thin solid lines correspond to $h = 0.95h_1$, the solid lines correspond to $h = h_1$, the thick solid lines correspond to $h = 1.05h$. For comparison we present analytical results for monomers (left panels) and dimers, $\mathcal{N} \to \infty$ (right panels) (empty symbols; triangles correspond to $h = 0.95h_1$, squares correspond to $h = h_1$, circles correspond to $h = 1.05h_1$). We also show by filled symbols the temperature dependence of the specific heat as it follows from equation (10) with $U = 1.57$ for the diamond chain and $U = 1.34$ for the square-kagomé lattice or from equation (18) for $\mathcal{N} \to \infty$ with $U = 1.10$ for the two-leg ladder.

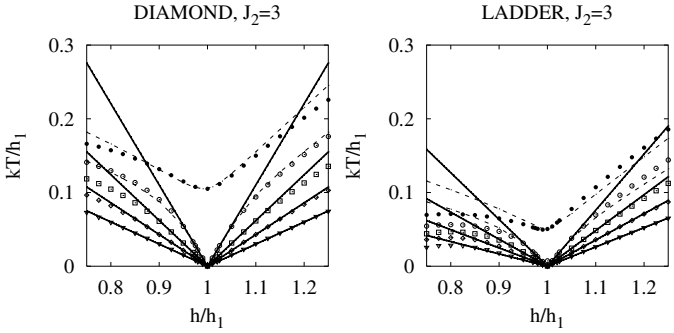

Fig. 8. Constant entropy curves as a function of magnetic field and temperature, $S(T, h, N)/kN = \text{const.}$, for the diamond chain with $N = 18$, $J_1 = 1$, $J_2 = 3$ (left) and the two-leg ladder with $N = 20$, $J_1 = 1$, $J_2 = 3$ (right). From bottom to top: $S(T, h, N)/kN = 0.05,\ 0.10,\ 0.15,\ 0.20,\ 0.25$. Solid lines correspond to analytical results which follow from equation (7) (left panel) or from equation (13) (right panel); broken lines correspond to analytical results for $S(T, h, N)/kN = 0.20,\ 0.25$ which follow from equation (10) with $U = 1.57$ (left panel) or from equation (18) for $\mathcal{N} \to \infty$ with $U = 1.10$ (right panel); symbols correspond to exact diagonalization data for finite spin systems.

II) extra spin states, which become irrelevant for larger N. The energy separation Δ for these systems with extra spin states we estimate to $\Delta \approx 0.9$ for the ladder ($J_1 = 1$, $J_2 = 2$, $N = 20$), $\Delta \approx 0.4$ for the kagomé-like chain I ($N = 18$), and $\Delta \approx 0.2$ for the kagomé-like chain II ($N = 20$). Therefore we obtain (see Fig. 6) a perfect agreement between the spin and the hard-core data only for very low temperatures, but realize a quantitative deviation already for $kT \approx 0.1$. Note that for the the kagomé-like chain II, the size $N = 20$ of the spin system corresponds to only $\mathcal{N} = 4$, and the finite size effects are clearly largest in this case.

From the experimental point of view the reported results manifest themselves most interestingly in a drastic change of the low-temperature specific heat, when the magnetic field passes the saturation field, and in the maximum of the isothermal entropy at saturation field leading to an enhanced magnetocaloric effect (for a general discussion of the magnetocaloric effect for quantum spin systems, see Ref. [12]). We illustrate that in Figures 7 and 8, where we present finite-lattice data for spin systems, but hard-core results for the thermodynamic limit to demonstrate that the discussed effects remain relevant for $N \to \infty$.

In Figure 7 we present the temperature dependence of the specific heat at three values of the external magnetic field, $h = 0.95h_1, h_1, 1.05h_1$, for several spin systems. Firstly, we note that within the hard-core object description the specific heat equals to zero at saturation field $h = h_1$. That is also observed in a certain range of low temperatures around zero for the diamond chain with $J_2 > 2J_1$, the square-kagomé lattice with $J_2 > J_1$ or the two-leg ladder with $J_2 > 2J_1$, but we do not observe the zero-value region of C/kN at low temperatures for the spin systems having extra spin states and low separation Δ. Secondly, we see that the specific heat in the vicinity of the saturation field (but $h \neq h_1$) has an extra low-temperature peak which is satisfactorily reproduced within the hard-core object lattice gas approach (compare lines and empty triangles and circles in Fig. 7). The hard-core description can be improved assuming a finite on-site energy parameter U (filled triangles and circles in Fig. 7). As it was already noticed in reference [8] in the context of the sawtooth chain and the kagomé lattice, the experimental observation of the low-temperature peak of the

specific heat can be a sign of highly degenerate localized magnon states.

Finally, we consider in Figure 8 adiabatic cooling processes, i.e. we show curves of constant entropy as a function of magnetic field and temperature. Again the exact diagonalization data for the diamond chain with $N = 18$, $J_1 = 1$, $J_2 = 3$ (left panel) and the two-leg ladder with $N = 20$, $J_1 = 1$, $J_2 = 3$ (right panel) are in a good agreement with the universal curves for monomers and one-dimensional dimers. Taking the data for spin systems, which show some asymmetry between $h > h_1$ and $h < h_1$, we observe, that an efficient cooling to very low temperatures can be achieved by an adiabatic demagnetization via lowering the magnetic field from above saturation till saturation.

5 Summary

We have presented a universal description of thermodynamic properties of a wide class of frustrated quantum spin antiferromagnets at low temperatures in the vicinity of the saturation field. The reason for that is a dominant contribution of highly degenerate localized magnon states to the partition function, which can be calculated using a hard-core object representation. We have provided exact diagonalization data to justify such a picture.

The spin systems hosting localized magnons can be grouped into different universality classes of hard-core lattice gases, namely gases of hard squares, hard hexagons, hard dimers or hard monomers. Comparing the analytical predictions with numerical data for finite spin systems we have found that the hard-core picture describes accurately the spin physics near the saturation field and at sufficiently low temperatures. Since other states of the spin system, not described by the hard-core model, become relevant as temperature grows, the hard-core description is less accurate, but it remains qualitatively correct at higher temperatures. The hard-core object lattice gas models may be improved by relaxing the hard-core constraint. Such an improvement breaks the universality, but provides a better quantitative agreement with exact diagonalization results for higher temperatures and larger deviations from the saturation field.

We emphasize that some peculiarities of the thermodynamic quantities arising due to the localized magnon states are of interest from the experimental point of view. Thus, the specific heat at the saturation field remains almost zero below a certain temperature whereas at fields slightly above/below the saturation field the specific heat exhibits a well-pronounced extra low-temperature peak. A frustrated spin system hosting localized magnons also exhibits a large magnetocaloric effect in the vicinity of the saturation field; similarly to an ideal paramagnet.

We thank T. Krokhmalskii for discussions on two-dimensional lattice gases of hard-core objects and A. Honecker and J. Schnack for a critical reading of the manuscript. The numerical calculations were performed using J. Schulenburg's *spinpack*. We also thank the DFG for the support (Project No. 436 UKR 17/13/05). One of the authors (O.D.) thanks the Abdus Salam International Centre for Theoretical Physics at Trieste, where a part of this work was carried out, for hospitality in the autumn of 2005.

References

1. G. Misguich, C. Lhuillier, in *Frustrated Spin Systems*, edited by H.T. Diep (World Scientific, Singapore, 2005), pp. 229–306
2. H.-J. Mikeska, A.K. Kolezhuk, in *Quantum Magnetism*, edited by U. Schollwöck, J. Richter, D.J.J. Farnell, R.F. Bishop, Lecture Notes in Physics, 645 (Springer, Berlin, 2004), pp. 1–83
3. J. Richter, J. Schulenburg, A. Honecker, in *Quantum Magnetism*, edited by U. Schollwöck, J. Richter, D.J.J. Farnell, R.F. Bishop, Lecture Notes in Physics, 645 (Springer, Berlin, 2004), pp. 85–153
4. J. Schnack, H.-J. Schmidt, J. Richter, J. Schulenburg, Eur. Phys. J. B **24**, 475 (2001)
5. J. Schulenburg, A. Honecker, J. Schnack, J. Richter, H.-J. Schmidt, Phys. Rev. Lett. **88**, 167207 (2002)
6. J. Richter, J. Schulenburg, A. Honecker, J. Schnack, H.-J. Schmidt, J. Phys.: Condens. Matter **16**, S779 (2004)
7. J. Richter, Fizika Nizkikh Temperatur (Kharkiv) **31**, 918 (2005) [Low Temperature Physics **31**, 695 (2005)]
8. M.E. Zhitomirsky, H. Tsunetsugu, Prog. Theor. Phys. Suppl. No. **160**, 361 (2005)
9. J. Richter, O. Derzhko, J. Schulenburg, Phys. Rev. Lett. **93**, 107206 (2004); O. Derzhko, J. Richter, J. Schulenburg, Physica Status Solidi (b) **242**, 3189 (2005)
10. O. Derzhko, J. Richter, Phys. Rev. B **72**, 094437 (2005)
11. O. Derzhko, J. Richter, Phys. Rev. B **70**, 104415 (2004)
12. M.E. Zhitomirsky, A. Honecker, J. Stat. Mech.: Theor. Exp. P07012 (2004)
13. M.E. Zhitomirsky, H. Tsunetsugu, Phys. Rev. B **70**, 100403(R) (2004)
14. K. Takano, K. Kubo, H. Sakano, J. Phys.: Condens. Matter **8**, 6405 (1996); H. Niggemann, G. Uimin, J. Zittartz, J. Phys.: Condens. Matter **9**, 9031 (1997); A. Honecker, A. Läuchli, Phys. Rev. B **63**, 174407 (2001); K. Okamoto, T. Tonegawa, M. Kaburagi, J. Phys.: Condens. Matter **15**, 5979 (2003); L. Čanová, J. Strečka, M. Jaščur, J. Phys.: Condens. Matter **18**, 4967 (2006)
15. N.B. Ivanov, J. Richter, Phys. Lett. A **232**, 308 (1997); J. Richter, N.B. Ivanov, J. Schulenburg, J. Phys.: Condens. Matter **10**, 3635 (1998); A. Koga, K. Okunishi, N. Kawakami, Phys. Rev. B **62**, 5558 (2000); J. Schulenburg, J. Richter, Phys. Rev. B **65**, 054420 (2002); A. Koga, N. Kawakami, Phys. Rev. B **65**, 214415 (2002)
16. T. Nakamura, K. Kubo, Phys. Rev. B **53**, 6393 (1996); D. Sen, B.S. Shastry, R.E. Walstedt, R. Cava, Phys. Rev. B **53**, 6401 (1996); V. Ravi Chandra, D. Sen, N.B. Ivanov, J. Richter, Phys. Rev. B **69**, 214406 (2004); G.C. Lau, B.G. Ueland, R.S. Freitas, M.L. Dahlberg, P. Schiffer, R.J. Cava, Phys. Rev. B **73**, 012413 (2006)
17. M.P. Gelfand, Phys. Rev. B **43**, 8644 (1991); F. Mila, Eur. Phys. J. B **6**, 201 (1998); A. Honecker, F. Mila, M. Troyer, Eur. Phys. J. B **15**, 227 (2000)
18. Ch. Waldtmann, H. Kreutzmann, U. Schollwöck, K. Maisinger, H.-U. Everts, Phys. Rev. B **62**, 9472 (2000)

19. P. Azaria, C. Hooley, P. Lecheminant, C. Lhuillier, A.M. Tsvelik, Phys. Rev. Lett. **81**, 1694 (1998)
20. R. Siddharthan, A. Georges, Phys. Rev. B **65**, 014417 (2002); P. Tomczak, J. Richter, J. Phys. A **36**, 5399 (2003); J. Richter, J. Schulenburg, P. Tomczak, D. Schmalfuß, e-print `arXiv:cond-mat/0411673`
21. P. Lecheminant, B. Bernu, C. Lhuillier, L. Pierre, P. Sindzingre, Phys. Rev. B **56**, 2521 (1997); Ch. Waldtmann, H.-U. Everts, B. Bernu, C. Lhuillier, P. Sindzingre, P. Lecheminant, L. Pierre, Eur. Phys. J. B **2**, 501 (1998); F. Mila, Phys. Rev. Lett. **81**, 2356 (1998); D.C. Cabra, M.D. Grynberg, P.C.W. Holdsworth, A. Honecker, P. Pujol, J. Richter, D. Schmalfuß, J. Schulenburg, Phys. Rev. B **71**, 144420 (2005)
22. J. Richter, J. Schulenburg, A. Honecker, D. Schmalfuß, Phys. Rev. B **70**, 174454 (2004)
23. S.E. Palmer, J.T. Chalker, Phys. Rev. B **64**, 094412 (2001); W. Brenig, A. Honecker, Phys. Rev. B **65**, 140407 (2002); J.-B. Fouet, M. Mambrini, P. Sindzingre, C. Lhuillier, Phys. Rev. B **67**, 054411 (2003)
24. H.-J. Schmidt, J. Phys. A **35**, 6545 (2002)
25. H.-J. Schmidt, J. Richter, R. Moessner, e-print `arXiv:cond-mat/0604649` in preparation
26. A. Honecker, private communication
27. R.J. Baxter, Exactly Solved Models in Statistical Mechanics (Academic Press, London, 1982)
28. F.H. Ree, D.A. Chesnut, Phys. Rev. Lett. **18**, 5 (1967); A. Bellemans, R.K. Nigam, J. Chem. Phys. **46**, 2922 (1967); L. Lafuente, J.A. Cuesta, J. Chem. Phys. **119**, 10832 (2003)
29. M.E. Zhitomirsky, H. Tsunetsugu, unpublished (2004)
30. T. Krokhmalskii, unpublished (2005)